Clim Dyn (2015) 44:897–906
DOI 10.1007/s00382-014-2181-x

The skill of atmospheric linear inverse models in hindcasting the Madden–Julian Oscillation

Nicholas R. Cavanaugh · Teddy Allen · Aneesh Subramanian · Brian Mapes · Hyodae Seo · Arthur J. Miller

Received: 10 September 2013 / Accepted: 14 May 2014 / Published online: 25 May 2014

Abstract A suite of statistical atmosphere-only linear inverse models of varying complexity are used to hindcast recent MJO events from the Year of Tropical Convection and the Cooperative Indian Ocean Experiment on Intraseasonal Variability/Dynamics of the Madden–Julian Oscillation mission periods, as well as over the 2000–2009 time period. Skill exists for over two weeks, competitive with the skill of some numerical models in both bivariate correlation and root-mean-squared-error scores during both observational mission periods. Skill is higher during mature Madden–Julian Oscillation conditions, as opposed to during growth phases, suggesting that growth dynamics may be more complex or non-linear since they are not as well captured by a linear model. There is little prediction skill gained by including non-leading modes of variability.

Keywords Madden–Julian Oscillation · Hindcast · Predictability · Linear inverse model · Tropical dynamics

N. R. Cavanaugh (✉) · A. Subramanian · A. J. Miller
Scripps Institution of Oceanography, University of California San Diego, 9500 Gilman Drive, La Jolla, CA 92093-0208, USA
e-mail: ncavanaugh@ucsd.edu

T. Allen · B. Mapes
Rosenstiel School of Marine and Atmospheric Science, University of Miami, Miami, FL, USA

H. Seo
Woods Hole Oceanographic Institution, Massachusetts Institute of Technology, Woods Hole, MA, USA

1 Introduction

The Madden–Julian Oscillation (MJO) is a large-scale zonally propagating atmospheric signal in tropical rainfall and related fields (Madden and Julian 1971) and is the dominant mode of intraseasonal variability in the tropics (Wheeler and Hendon 2004, hereafter WH04). The MJO modulates high-frequency weather, both in the tropics and extra-tropics through teleconnections (Wallace and Gutzler 1981; Ferranti et al. 1990; Maloney 2000; Matthews and Meredith 2004; Cassou 2008; Roundy and Gribble-Verhagen 2010; Martin and Schumacher 2011), and has also been shown to affect longer timescale climate variability, for example the El Niño Southern Oscillation (Lau and Chan 1985; Lau and Chan 1988; Kessler and Kleeman 2000; Zhang 2001; Subramanian et al. 2011). Many studies have suggested that the MJO may provide an avenue for predictability beyond the traditional 10-day limit (Waliser et al. 2003; Reichler and Roads 2005). Verification of predictions may be done in the space of the real-time multivariate MJO index (RMM, see WH04), comprising the leading two maximum covariance or empirical orthogonal function (EOF) modes of combined tropical 200 and 850 mb zonal wind (u200 and u850, respectively) and outgoing long-wave radiation (OLR) in the intraseasonal band. Bivariate correlations of forecasts and verifications of these two modes, and root-mean-squared error (RMSE) metrics proposed by Lin et al. (2008), make a well-accepted set of verification metrics (Gottschalck et al. 2010) which we will use here. Specific details of the metrics and their interpretations can be found in those papers.

MJO hindcast skill studies utilizing high-dimensional numerical models have increased in recent years (Zhang et al. 2013). These hindcasts are usually produced for time

periods coinciding with large, coordinated MJO research missions, such as the Year of Tropical Convection (YoTC, Waliser and Moncrief 2007) and Cooperative Indian Ocean Experiment on Intraseasonal Variability/Dynamics of the Madden–Julian Oscillation (CINDY/DYNAMO, Yoneyama et al. 2013). Several statistical forecast studies relevant to the MJO have been reported. Simple extrapolation by Fourier filtered zero-padded longitude-time sections (Wheeler and Weickmann 2001) is one approach. Many kinds of covariance models have also been tried, including Principal Oscillation Patterns (POP, von Storch and Xu 1990); a singular value decomposition forecasting technique (Waliser and Jones 1999); and lagged regressions on EOFs of OLR and circulation indices, sometimes bandpass filtered (Lo and Hendon 2000; Jones et al. 2004). Maharaj and Wheeler (2005) and Jiang et al. (2008) are regression models based on the RMM1 and RMM2 EOFs (convenient for verification). Kang and Kim (2010) summarize the predictability from a collection of statistical and dynamical models, but the variety of skill tests utilized across past studies complicates comparisons.

The linear inverse model (LIM, Penland and Magorian 1993) constitutes the least complex form of a reduced stochastic-dynamic climate model (Majda et al. 2009) and has been used for diagnostics and prediction in several studies of the atmosphere (e.g., Winkler 2001; Newman et al. 2003; Pegion and Sardeshmukh 2011) and coupled atmosphere–ocean system (Newman et al. 2009). These LIMs have been shown to have comparable predictive capability to global circulation models, even though they have far fewer degrees of freedom. Pegion and Sardeshmukh (2011) compared a simple atmospheric LIM to coupled atmosphere–ocean numerical models to conclude that there is room for hindcast skill improvement in tropical climate prediction specifically.

In this paper, we explore the use of atmospheric LIMs in the established context of MJO forecast verification. We will see that simple stochastic-dynamic representations can provide hindcast skills comparable to other statistical approaches and to some GCMs, and offer useful informed hypotheses about MJO dynamics along the way. Section 2 introduces LIM theory briefly, and establishes the subset of models used in this analysis. Section 3 shows LIM hindcast skill for the DYNAMO period, two YoTC MJO events, and a ten-year continuous hindcast period. Finally, we conclude with a discussion and directions for future research.

2 Model details and methodology

Using the notation of Newman et al. (2009), the fundamental assumption underpinning LIM is that the governing dynamics of the system under consideration can be modeled as

$$\frac{d\mathbf{x}}{dt} = \mathbf{L}\mathbf{x} + \xi \tag{1}$$

where $\mathbf{x}$ represents an appropriate system state vector, $\mathbf{L}$ is a linear operator matrix, and ξ is a vector of stochastic temporally white but spatially structured Gaussian noise. In a system where (1) is stable, lag-covariance matrices decay exponentially, so $\mathbf{L}$ can be estimated from observational estimates of covariance matrices $\mathbf{C}(\tau)$ where $C_{ij}(\tau) = \langle \mathbf{x}_i(t+\tau)\mathbf{x}_j(t) \rangle$ evaluated at any fixed lag, where subscripts i and j correspond to covarying observational time series, as well as the rows and columns of $\mathbf{C}$, respectively. For some chosen lead-time τ_0, $\mathbf{L}$ is estimated as $\mathbf{L} = \tau_0^{-1} \ln\left[\mathbf{C}(\tau_0)\mathbf{C}^{-1}(0)\right]$. Eq. 1 can then be solved for analytically: $\mathbf{x}(t+\tau) = \mathbf{G}(\tau)\mathbf{x}(t) + \varepsilon$ where $\mathbf{G}(\tau) = \exp(\mathbf{L}\tau)$ represents the decaying, predictable signals at forecast lead time τ and ε is a random variable vector with covariance $\mathbf{E}(\tau) = \mathbf{C}(0) - \mathbf{G}(\tau)\mathbf{C}(0)\mathbf{G}^{-1}(\tau)$. The random vector ε is multivariate Gaussian and grows as a function of τ regardless of the initial condition at time t and can also be estimated from a suitable set of hindcast errors. More comprehensive overviews of LIM can be found in Penland (1989) and Penland and Sardeshmukh (1995) and its application in the tropics in Newman et al. (2009) and Pegion and Sardeshmukh (2011).

The data channels which constitute $\mathbf{x}$ may be time series of variables in physical space or principal component (PC) time series of EOFs of the data comprising the desired forecast space. The diagonal components of $\mathbf{L}$ express the individual decay of each of the predicted variables, whereas the off-diagonal components of $\mathbf{L}$ represent modal interactions (if $\mathbf{x}$ is in a mode basis) or propagation (if $\mathbf{x}$ is in a spatial basis). Imaginary $\mathbf{L}$ components describe oscillations (e.g. in the POP model of Penland 1989). After fitting $\mathbf{L}$, the residual noise ξ can be obtained. Its EOFs describe leading spatially coherent patterns of stochastic forcing necessary to reproduce the observed data, and thus might be interpretable in terms of sources of high-frequency (spectrally white) turbulent or chaotic energy in nature, which are being parameterized in the LIM as noise (see Penland and Matrosova 1994).

In this study, we chose a reduced climate state vector $\mathbf{x} = [\mathbf{W}\ \mathbf{O}]^{\mathrm{T}}$, where $\mathbf{W}$ is the PCs associated with some number of leading EOFs of concatenated 850 and 200 mb u- and v- wind anomalies from the National Centers for Environmental Prediction Climate Prediction Center (NCEP/CPC) Reanalysis 2 (Kanamitsu et al. 2002), and $\mathbf{O}$ is some number of leading PCs of OLR anomalies from the National Oceanic and Atmospheric Administration (NOAA) Interpolated OLR dataset (Liebmann and Smith

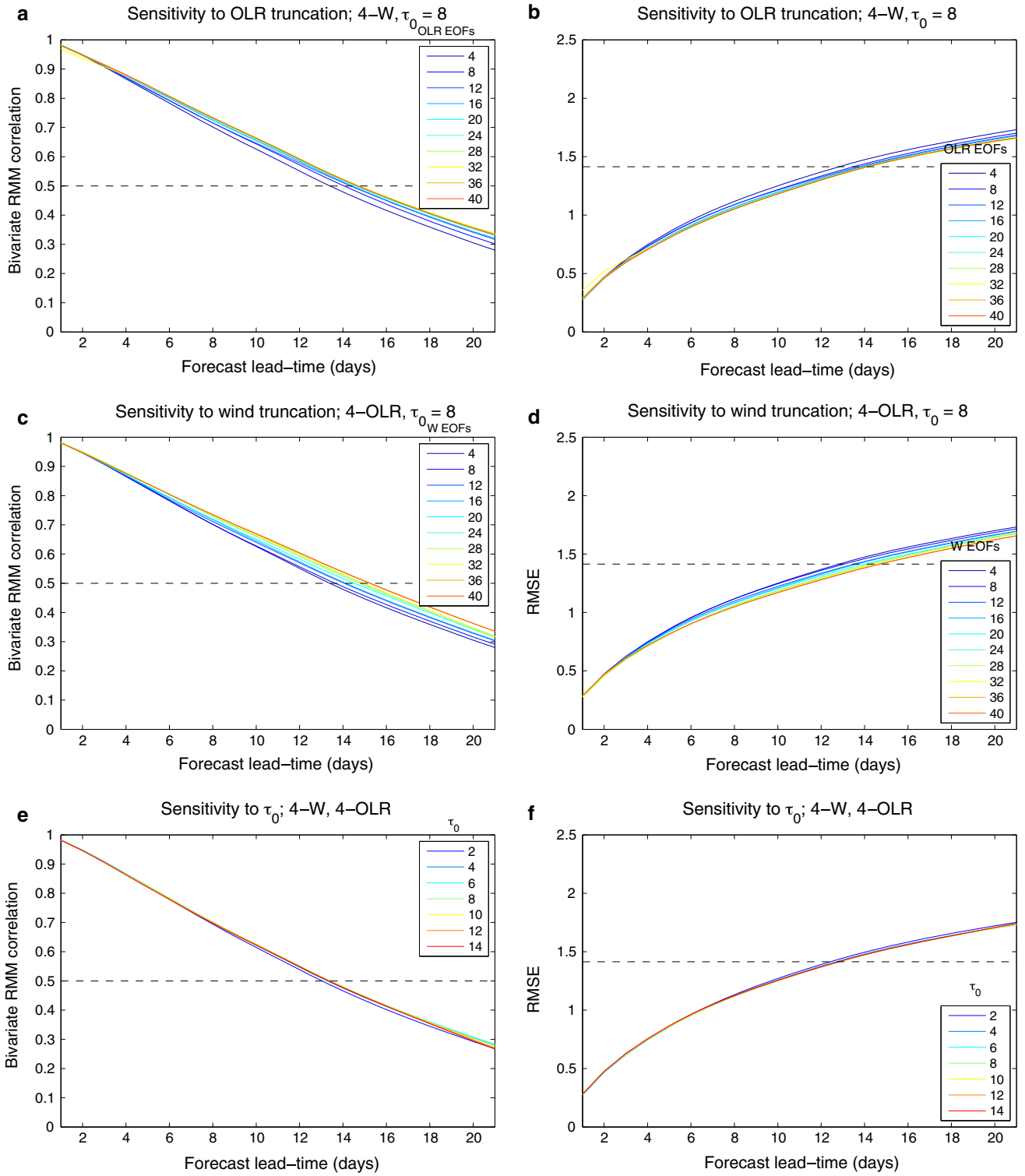

Fig. 1 Bivariate correlation (*left column*) and RMSE (*right column*) for LIM suite hindcasts over the 2000–2009 validation period. Subplots **a**–**b** show MJO skill sensitivity to OLR truncation. Subplots **c**–**d** and **e**–**f** are the same as a–b except for winds and τ_0 sensitivity, respectively

1996). Both datasets are used from 1980 to 2012. To define these EOF-PC pairs, all variables were first truncated to T21 resolution, transformed to a Gaussian grid from 25°S to 25°N, and smoothed with a 7-day running mean filter, as in Newman et al. (2009). Unsmoothed data withheld from the training set are projected onto the leading EOFs from

the smoothed data to produce out-of-sample hindcasts which do not utilize any future data and are therefore valid as daily predictions. These smoothing techniques were selected to attenuate unpredictable (high-frequency) signals that can corrupt LIM dynamics through aliasing, but in this case MJO hindcast skills are largely insensitive to these filtering choices since EOF shapes are dominated by large-scale and low-frequency variability even in daily fine-grid data. LIMs constructed directly from unfiltered data EOFs provide similar predictions and corroborate the results of this study.

Four-week tropical hindcasts were initiated for each day Jan 1, 1999–Dec 31, 2012, for each combination of [4, 8, 12, …, 40] EOFs of **W**, [4, 8, 12, …, 40] EOFs of **O,** and $\tau_0 = [2, 4, \ldots, 14]$, resulting in 700 models. LIM hindcasts are cross-validated by excluding the data during the year in which the hindcast is constructed when fitting the model. Model hindcasts were transformed back into physical space and then projected onto the WH04 RMM indices (which only involve zonal winds and OLR) for skill verification.

3 Results

The lowest complexity model is chosen as a baseline for comparison with a training lag time of eight days: four wind EOFs and four EOFs of OLR in the 25N-25S belt are included, summarized as 4-**W** 4-**O**, and $\tau_0 = 8$. Figure 1 shows bivariate correlation (left column) and RMSE (right column) for the Jan 1, 2000–Dec 31, 2009 interval. Overall, the all-season ten-year MJO hindcast skill is quite consistent across all our models. Decorrelation times, measured as the time when correlation falls below 0.5 (Gottschalck et al. 2010), are about 14–16 days. Similarly, RMSE skill, as measured by the lead-time at which the RMSE crosses $\sqrt{2}$ (Lin et al. 2008; Vitart et al. 2010) across all models is also about 14 days.

Figure 1a, b shows MJO skill sensitivity to OLR truncation. All conclusions are consistent in both the correlation and the RMSE skill metrics. Hindcast skill improves slightly by increasing the number of OLR predictors included in the model (Fig. 1a, b) until the skill level saturates at a high complexity. Similarly, including more **W** modes increases model skill essentially monotonically, particularly after about 7 days of hindcast (Fig. 1c, d), but with similar forecast skill prior to 7 days (when lower complexity therefore suffices), again before the skill level saturates at a high complexity. MJO hindcast skill is insensitive to τ_0 (Fig. 1e, f), indicating smoothly and exponentially decaying lag-covariances, as assumed in the LIM theory (Penland and Sardeshmukh 1995). These results suggest that there is little linear MJO predictability (about 1–2 day skill extension) associated with non-leading EOFs, and that under this model construction, prediction skill is independent of the training lead-time. Sensitivities for models composed of unfiltered EOFs are slightly increased, however, the main conclusions remain consistent with those presented here.

Figures 2a-d show the structure of the first four EOFs of OLR used in the model. The first two EOFs show similar equatorially symmetric patterns roughly orthogonal to each other. The first pattern shows a pattern of low OLR in the central Pacific region when the principal component is positive while the second reveals a pattern with lowest OLR in the Western Pacific region corresponding to a positive PC value. The third and fourth EOFs of OLR have both equatorial and off-equatorial structures in the West Pacific and reveal patterns with higher wavenumbers (wavenumbers 2–3) in the equatorial region.

Spatial patterns of the first four EOFs of the combined 850 and 200 mb winds are shown in Fig. 3a-h. Shading indicates regions of convergence and divergence with blue indicating regions of divergence and red indicating regions of convergence corresponding to a positive PC value. The first EOF of the winds at 850 and 200 mb (Figs. 3a-b) show regions of strong high-level convergence and low-level divergence over the Western Pacific Ocean region. This region also corresponds to the concentrated variability in OLR highlighted by the first pair of EOFs of OLR. The second, third and fourth EOFs of winds reveal off-equatorial regions of increased variability in divergence especially in the region of the Inter-Tropical Convergence Zone.

Leading EOFs of both OLR and the combined winds have broad spectral peaks in the intraseasonal and interannual band (not shown). Interactions of these modes, as quantified by the matrix of interaction coefficients $\mathbf{G}(\tau)$ (demonstrated in Fig. 4 as $\|\mathbf{G}(\tau = 7, 14, 21)\|$), confirm that the magnitudes of the interactions between the leading EOFs (Fig. 4, α-δ) are dominant in comparison to interactions between the non-leading EOFs, which tend to decay toward zero for lesser modes of variability, particularly for large τ. Interestingly, interaction coefficients $\mathbf{G}_{i<j}(\tau)$ for the **OO** matrix block are generally of greater magnitude than coefficients $\mathbf{G}_{i>j}(\tau)$, indicating that the upscale interactions from modes of lower variability to those of higher variability play a more dominant role than those of downscale interactions in intraseasonal forecasts.

Figure 5a, b shows bivariate correlation and RMSE for multiple hindcast intervals from the best-performing model (24-**W**, 32-**O**, $\tau_0 = 6$) based on bivariate correlation after 10 days over the whole 2000–2009 period. Results are comparable to the numerical model scores for the YoTC hindcast period of Oct. 10, 2009-Nov. 25, 2009 and Dec. 10, 2009-Jan. 25, 2010 (Klingaman et al. 2014, personal communication) and the DYNAMO hindcast period of

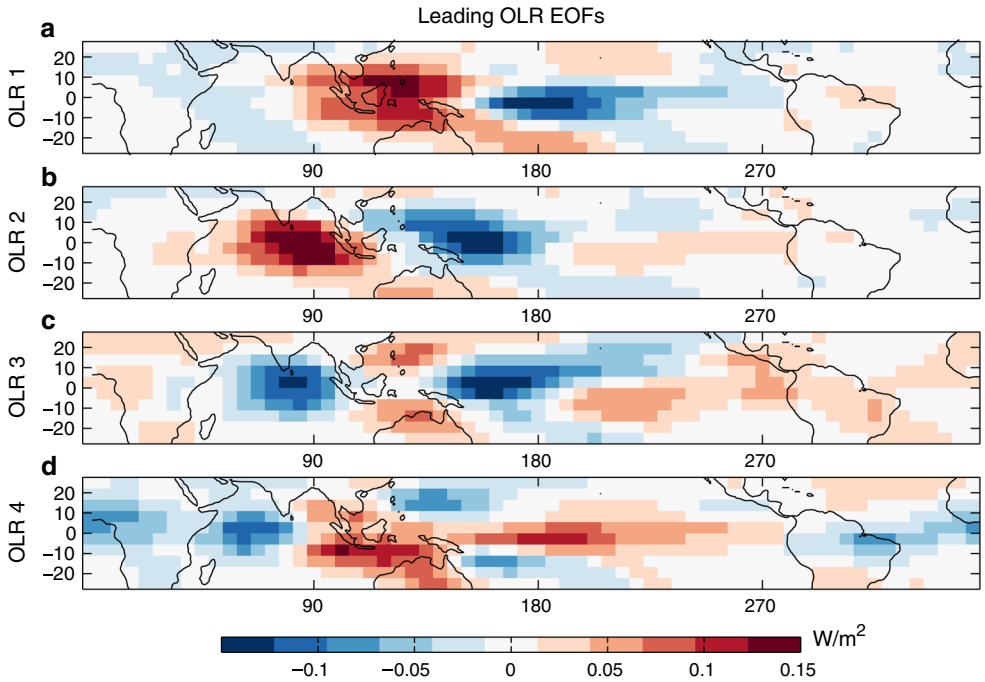

Fig. 2 First four leading EOFs of tropical OLR. **a** Represents 8.3 % of the smoothed variance field. **b** 5.5 %. **c** 3.6 %. **d** 3.0 %

Sept. 1, 2011-Mar. 31, 2012 (Zhang et al. 2013, Fig. 2b). Useful bivariate correlation skill ranges during DYNAMO for numerical models are approximately 8–15+ days, and approximately 8–20+ days for YoTC. LIM hindcast skill for each comparable time period is on the low end of the dynamical model intercomparisons, but within the model spread, for both correlation and RMSE. This is particularly true during the DYNAMO period, where LIM skill is ~18 days. MJO skill scores are broken out for periods where the hindcast initialization date has a combined RMM amplitude of <1 (weak), $1 < \|\text{RMM}\| < 2$ (moderate), and $2 < \|\text{RMM}\|$ (strong). LIM underperforms compared to overall hindcast skill during weak MJO conditions as indicated by rapidly decorrelating hindcasts, however performance is markedly improved for moderate and strong MJO hindcasts (Fig. 5a) for each time period relative to hindcasts initialized from weak MJOs. Figure 5c, d shows bivariate correlation and RMSE separated by MJO phase at model initialization for the 2000–2009 period. LIM performance is relatively poor during phases 1, 2, and 6, with prediction skill to 14 days. Prediction during other phases is extended to between 15 and 19 days for bivariate correlation.

Figure 6 shows MJO hindcast propagation for the YoTC E case, Oct 10, 2009-Nov 25, 2009 for the best-performing model. The YoTC E case is selected since both the behavior of observations and its hindcasts most clearly illustrate the essential performance features of LIM, which are common across many MJO events, as well as the inability of LIM to capture (perhaps nonlinear) deviations from a smoothly propagating MJO evident in this particular event. Figure 6a shows multiple 3-week hindcasts initialized every 7 days over the same MJO event. Model initialization RMM values do not perfectly coincide with observation RMMs due to our EOF truncation and filtering choices. LIM forecasts are poor during the weak and moderate stages of MJO initiation, which correspond to times preceding amplitude errors that grow rapidly. Figure 6a shows rapidly intensifying amplitude errors during MJO initiation, which are consistent with information from Fig. 5c and d that highlight the relatively poor performance of MJO hindcasts during phases 1 and 2. This result indicates that rapid MJO initiation depends on either non-linear phenomena (e.g. Straub 2013; Kemball-Cook and Weare 2001) and/or processes, such as air-sea interaction in the Indian Ocean (Yoneyama et al. 2013) perhaps, with no linear projection on the set of current model variables in the historical training data. Once the MJO has reached a mature amplitude, however, hindcasts performance improves both in propagation speed and amplitude.

Figure 6b shows a series of one-week lead-time hindcasts. The nature of this plot is that each hindcast day is initialized one-week prior and the hindcast plot responds as it 'learns' of MJO initiation information. In this sense, the LIM hindcast tends to mimic MJO behavior when it incorporates the observed MJO state at the constant lead-time lag. For example, the LIM produces a stalled MJO around October 30 (index date 20 on Fig. 6b) since during

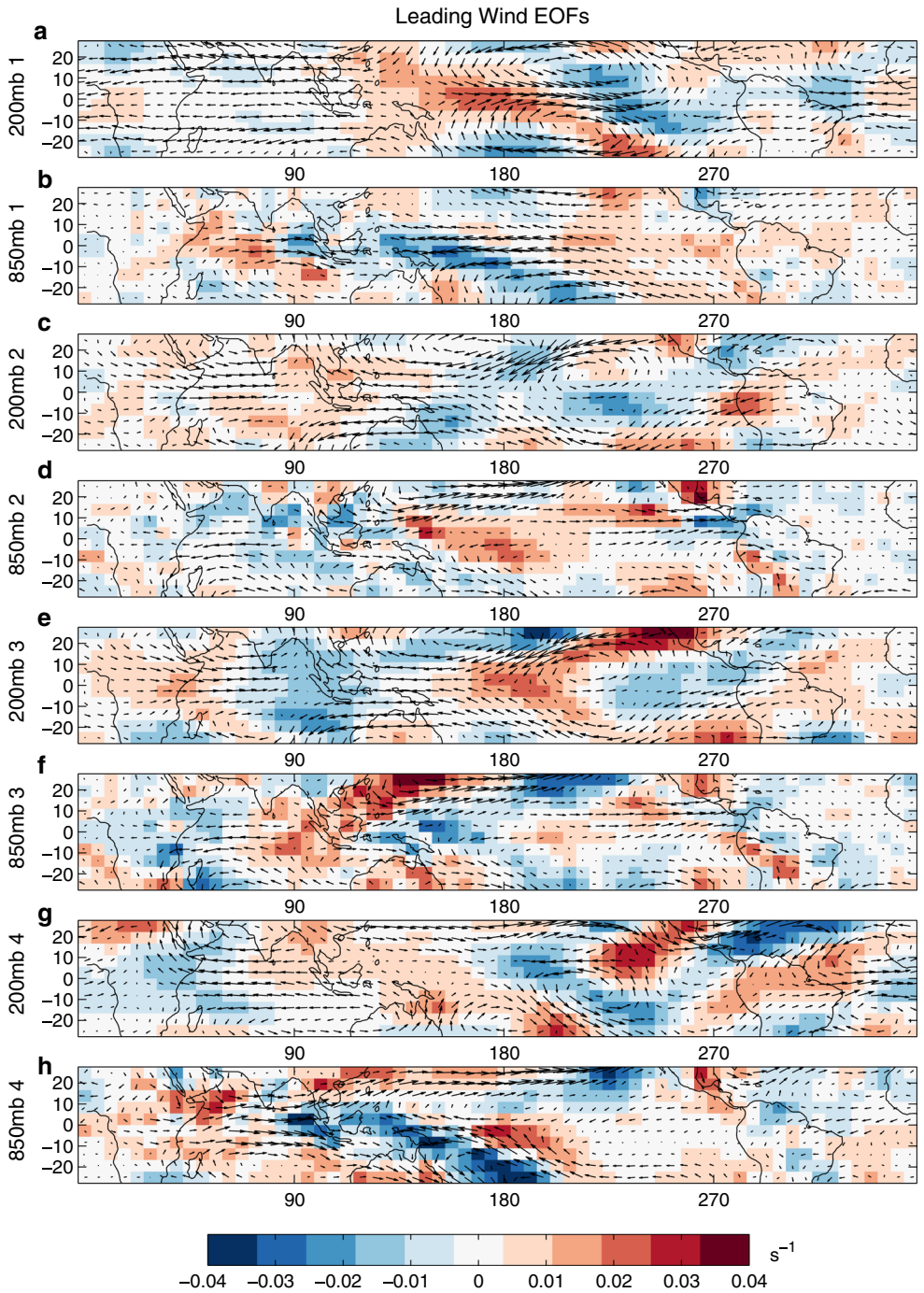

Fig. 3 Same as Fig. 2 for combined u200, u850, v200, and v850. Winds are plotted as vector fields, and magnitudes are shaded as 2-dimensional divergence fields. **a**, **b** Represents 6.9 % of the smoothed combined wind fields. **c**, **d** 4.2 %. **e**, **f** 3.0 %. **g**, **h** 2.4 %

the initiation day, October 23 (index 13 on Fig. 6b), the MJO was stalled. The failure of LIM to capture the stalling MJO behavior indicates that this YoTC E specific MJO initiation feature is inconsistent with linearized historical observations. Model behavior in these hindcast plots is typical and is similar for other MJO events observed during the YoTC and DYNAMO time periods (not shown).

4 Concluding remarks

This paper presents hindcast skill specific to MJO for a suite of LIMs composed of OLR and 200 and 850 mb winds over multiple intervals from 2000 to 2012. Results show that LIM skill is on the low end of current full-physics numerical models, but within the model spread for

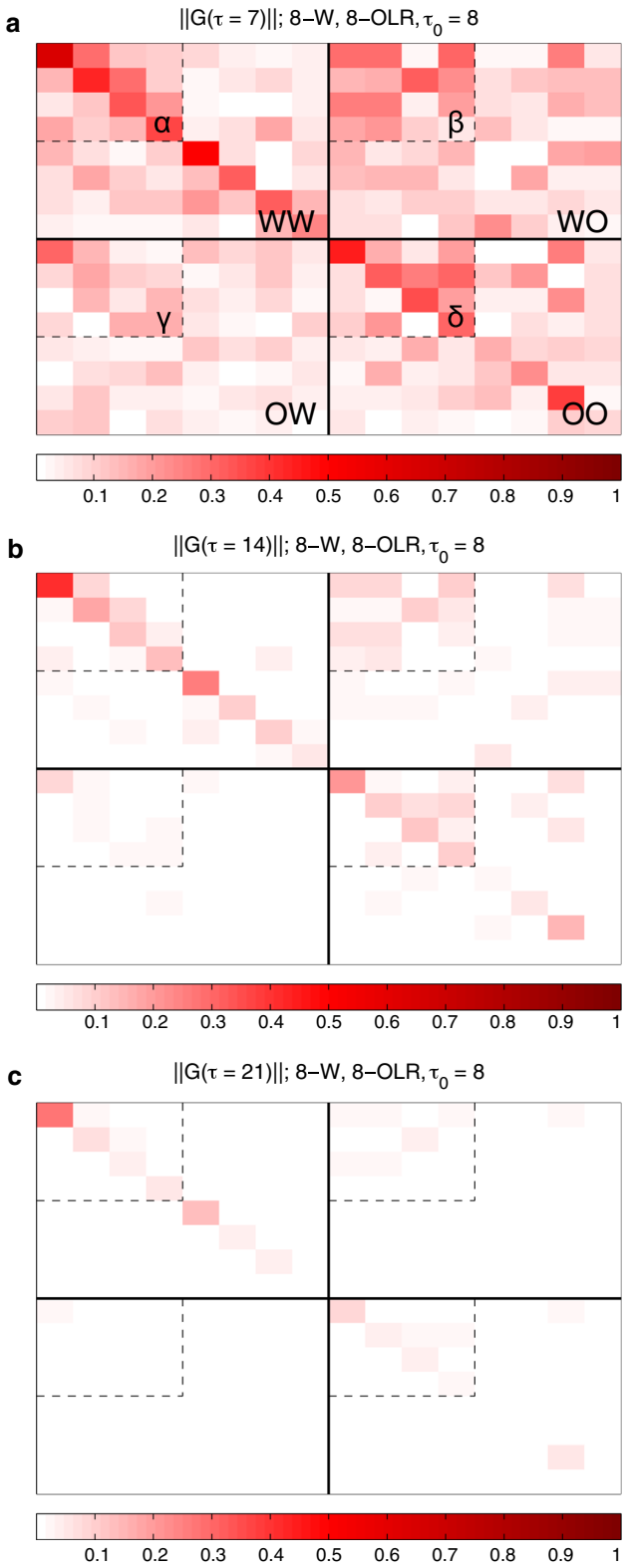

◀**Fig. 4** Magnitude of the modal interaction forecasting coefficients for the 8-**W** 8-**O** $\tau_0 = 6$ model at **a** $\tau = 7$ days, **b** $\tau = 14$ days, and **c** $\tau = 21$ days. The **WW** submatrix summarizes the magnitude of wind pattern interactions, **OO** summarizes OLR interactions, with cross-interactions **OW** and **WO** in the *bottom left* and *top right*, respectively, delineated by solid lines. Submatrices α-δ, delineated by dashed lines, summarize interactions amongst the first four EOFs of each (combined) field. *Rows* and *columns* are oriented as increasing from the upper left

bivariate correlation and RMSE during two comparison periods. This study highlights that these extremely simple empirical models perform competitively with GCMs at the low-end of the skill spread in MJO hindcasts. The LIMs presented here also perform competitively with other MJO statistical forecasting techniques, but are designed to reproduce full spatial fields of tropical variability, making them more comparable to numerical model output. We've chosen here to focus on skill related to the RMM indices to maximize the relevancy in the MJO community. Very little additional prediction skill is gained through the inclusion of more modes of variability, which in this case suggests that the simplest LIMs are likely most appropriate for MJO prediction, however the more complex LIMs may be useful toward achieving other goals, such as forecasting higher wavenumber features. This study also provides a forecast performance baseline for comparison with other forecast methodologies, particularly if only a short hindcast or observation period is available. Lastly, the analytical noise solution ε provides the statistics of an "infinite"-member ensemble forecast that may be used for uncertainty quantification at a much lower computational cost than producing large GCM ensembles to sample the uncertainty space.

The LIM performs particularly well during mature stages of the MJO. This suggests either that the LIM formulations presented here are missing key components of MJO initiation and amplification that are not linearly related to **x** or that MJO amplification marks a period of dominantly non-linear deviation from an otherwise more linear system which may be captured by better performing numerical models. Alternately, smoothly propagating mature MJO events whose amplitudes and phase speeds are well captured by LIM suggest that at maturity, MJO propagation behaves as a more linear system of traveling waves. Prediction skill during the YoTC events is lower than that during the DYNAMO and 2000–2009 validation periods, however this behavior may be a product of the short YoTC validation period.

There are many possible extensions to the LIMs presented here. Kondrashov et al. (2013) investigated the use of a quadratic inverse model of RMMs for MJO forecasting, which produce similar hindcast skill to our models. This is perhaps because the dominant quadratic terms are two orders of magnitude smaller than the linear coefficients (Kondrashov et al. 2013, supplementary material) and that there is at least some predictability beyond the RMMs which is captured by our models. That same study,

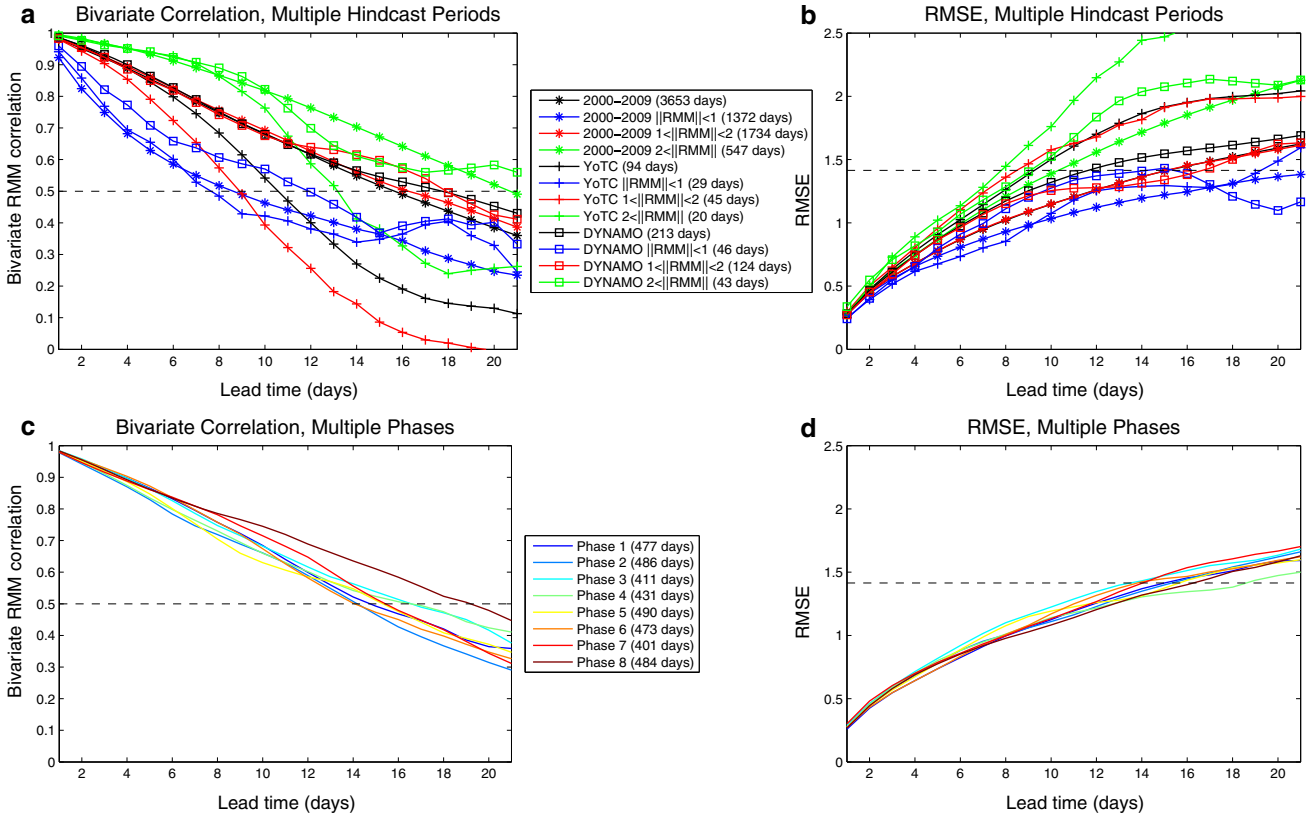

Fig. 5 Bivariate correlation (*left column*) and RMSE (*right column*) for 24-**W** 32-**O** $\tau_0 = 6$ LIM hindcasts. Subplots **a**, **b** show MJO skill over multiple time periods, DYNAMO, YoTC, and 2000–2009, separated additionally by their RMM amplitude performance. Subplots **c**, **d** show hindcast skill over the 2000–2009 time period separated by MJO phase. The DYNAMO performance in (**a**) is directly comparable to Zhang et al. (2013) Fig. 2b. YoTC performance is directly comparison to forthcoming figures in Klingaman et al. (in preparation). The number of sample days is summarized in the figure legends

however, achieved large hindcast skill improvements by training the model noise component only from time periods when the historically observed dynamics were similar to those observed at the hindcast initiation with so called past-noise forecasting. Another possible extension is to add a seasonally cyclostationary time-dependence, originally proposed by OrtizBevia (1997), by conditioning $\mathbf{L}$ and ξ on the time of the year either as piecewise linear or subject to a continuous empirical model. Previous studies have constructed seasonal LIMs (e.g., Winkler 2001; Newman et al. 2003; Pegion and Sardeshmukh 2011) and have achieved marginal skill increases over an all-season LIM. Ocean–atmosphere coupled LIMs may also add realism, but are unlikely to yield additional MJO hindcast skill due to the nearly uncoupled nature of the ocean and atmosphere at subseasonal timescales (Newman et al. 2009). Since our all-season LIM does not perform equally well at all amplitudes and phases of the MJO, it is possible that an MJO behavior-, amplitude- or phase-dependent LIM, resulting in a piecewise-stationary linear model, could yield large increases in MJO forecast skill, provided any hindcast stitching procedures do not produce amplifying errors and that the observed model skill deficiencies are not merely manifestations of the intrinsic predictability of the tropical atmosphere itself.

Lastly, it is well known that linear stochastic models with Gaussian white noise produce Gaussian forecasts, whereas high-frequency climate statistics are markedly non-Gaussian (Perron and Sura 2013, Cavanaugh and Shen 2014). An alternative mode reduction strategy, strategic choice of additional independent observable inputs containing MJO precursor and dynamics information, and/or augmentation of the system with correlated additive and multiplicative noise, suggested by Sura et al. (2005), may improve forecasts by accounting for more aspects of variability, while maintaining the simplicity of a linear stochastic framework.

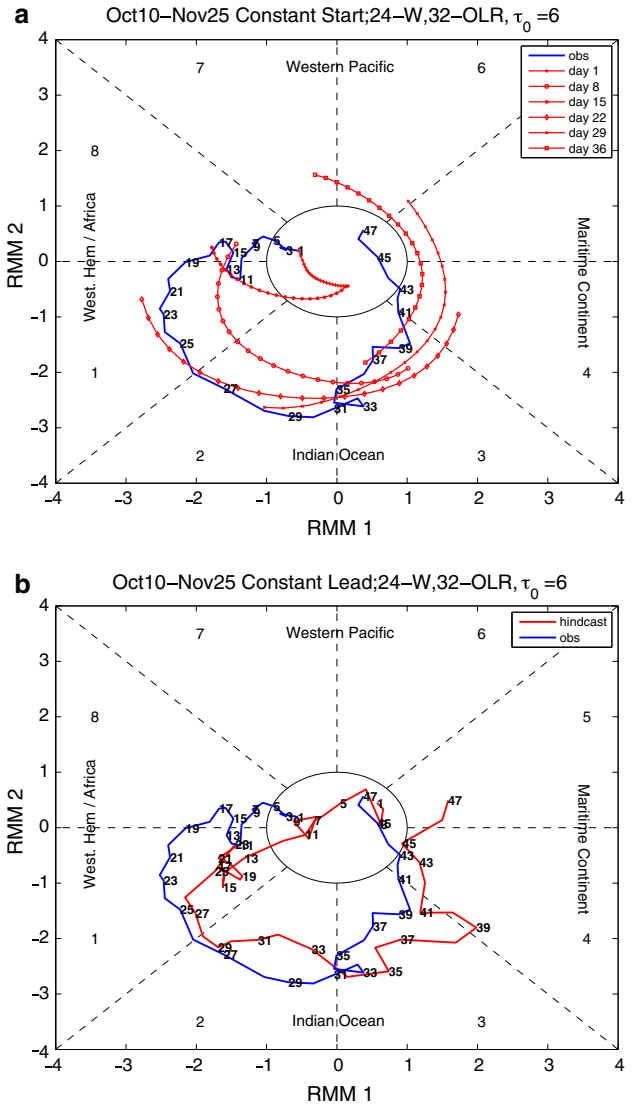

Fig. 6 **a** Multiple 3-week hindcasts for the YoTC E MJO initialized at multiple days over the MJO event. **b** Constant one-week lead-time forecast of the YoTC E MJO. Models are initialized with the EOF truncated observation data at hindcast-day 0 and trained with EOF truncated observation data which does not include the year in which the hindcast was made. Numbers located near plotted lines indicate days into the forecast period

Acknowledgments This material is based partly upon work supported by the National Science Foundation under Grant No. 0731520. We also gratefully acknowledge funding from ONR (Grants N00014-10-1-0541, N00014-13-1-0139, and N00014-13-1-0704) and NSF (OCE-0960770). We would like to thank Prashant Sardeshmukh, Cecile Penland, and Mathew Newman for conversations regarding LIM. Allen would like to thank Kathy Pegion of NOAA for her time and discussions towards understanding the LIM framework and its applications. We greatly appreciate the insightful comments of the four reviewers, whose input greatly enhanced the quality of this manuscript. In addition, Allen is grateful for the Wallace Fellowship administered by The University of Miami that helped to foster collaborative efforts among the authors.

References

Cassou C (2008) Intraseasonal interaction between the Madden–Julian Oscillation and the North Atlantic Oscillation. Nature 455:523–527. doi:10.1038/nature07286

Cavanaugh N, Shen SSP (2014) Northern hemisphere climatology and trends of statistical moments documented from GHCN-daily surface air temperature station data from 1950–2010. J Clim. doi:10.1175/JCLI-D-13-00470.1

Ferranti L, Palmer T, Molteni F, Klinker E (1990) Tropical-extratropical interaction associated with the 30–60 Day oscillation and its impact on medium and extended range prediction. J Atmos Sci 47:2177–2199

Gottschalck J, Wheeler M, Weickmann K et al (2010) A framework for assessing operational Madden–Julian oscillation forecasts: a CLIVAR MJO working group project. Bull Am Meteorol Soc 91:1247–1258. doi:10.1175/2010BAMS2816.1

Jiang X, Waliser DE, Wheeler MC et al (2008) Assessing the skill of an all-season statistical forecast model for the Madden–Julian Oscillation. Mon Weather Rev 136:1940–1956. doi:10.1175/2007MWR2305.1

Jones C, Carvalho L, Higgins RW et al (2004) A statistical forecast model of tropical intraseasonal convective anomalies. J Clim 17:2078–2095

Kanamitsu M, Ebisuzaki W, Woollen J et al (2002) NCEP–DOE AMIP-II Reanalysis (R-2). Bull Am Meteorol Soc 83:1631–1643. doi:10.1175/BAMS-83-11-1631

Kang I-S, Kim H-M (2010) Assessment of MJO Predictability for boreal winter with various statistical and dynamical models. J Clim 23:2368–2378. doi:10.1175/2010JCLI3288.1

Kemball-Cook S, Weare B (2001) The onset of convection in the Madden–Julian Oscillation. J Clim 14:780–793

Kessler W, Kleeman R (2000) Rectification of the Madden–Julian Oscillation into the ENSO cycle. J Clim 13:3560–3575

Klingaman NP, Woolnough SJ, Jiang X et al (2014) Vertical structure and diabatic processes of the Madden-Julian oscillation: linking hindcast fidelity to simulated diabatic heating and moistening. J Geophys Res (to be submitted)

Kondrashov D, Chekroun MD, Robertsona W, Ghil M (2013) Low-order stochastic model and "past-noise forecasting" of the Madden–Julian Oscillation. Geophys Res Lett 40:5305–5310. doi:10.1002/grl.50991

Lau K, Chan P (1985) Aspects of the 40–50 Day oscillation during the northern winter as inferred from outgoing longwave radiation. Mon Weather Rev 113:1889–1909

Lau K, Chan P (1988) Intraseasonal and interannual variation of the tropical convection: a possible link between the 40–50 day oscillation and ENSO? J Atmos Sci 45:506–521

Liebmann B, Smith C (1996) Description of a complete (interpolated) outgoing longwave radiation dataset. Bull Am Meteorol Soc 77:1275–1277

Lin H, Brunet G, Derome J (2008) Forecast skill of the Madden–Julian Oscillation in two Canadian atmospheric models. Mon Weather Rev 136:4130–4149. doi:10.1175/2008MWR2459.1

Lo F, Hendon H (2000) Empirical extended-range prediction of the Madden–Julian Oscillation. Mon Weather Rev 128:2528–2543

Madden R, Julian P (1971) Detection of a 40–50 day oscillation int he zonal wind in the tropical Pacific. J Atmos Sci 28:702–708

Maharaj EA, Wheeler MC (2005) Forecasting an index of the Madden-oscillation. Int J Climatol 25:1611–1618. doi:10.1002/joc.1206

Majda AJ, Franzke C, Crommelin D (2009) Normal forms for reduced stochastic climate models. Proc Natl Acad Sci USA 106:3649–3653. doi:10.1073/pnas.0900173106

Maloney ED (2000) Modulation of hurricane activity in the Gulf of Mexico by the Madden–Julian Oscillation. Science 287:2002–2004. doi:10.1126/science.287.5460.2002

Martin ER, Schumacher C (2011) Modulation of Caribbean precipitation by the Madden–Julian Oscillation. J Clim 24:813–824. doi:10.1175/2010JCLI3773.1

Matthews AJ, Meredith MP (2004) Variability of Antarctic circumpolar transport and the Southern Annular Mode associated with the Madden–Julian Oscillation. Geophys Res Lett. doi:10.1029/2004GL021666

Newman M, Sardeshmukh P, Winkler C, Whitaker JS (2003) A study of subseasonal predictability. Mon Weather Rev 131:1715–1732

Newman M, Sardeshmukh PD, Penland C (2009) How important is air–sea coupling in ENSO and MJO evolution? J Clim 22:2958–2977. doi:10.1175/2008JCLI2659.1

OrtizBevia M (1997) Estimation of the cyclostationary dependence in geophysical data fields. J Geophys Res 102:13473–13486

Pegion K, Sardeshmukh PD (2011) Prospects for improving subseasonal predictions. Mon Weather Rev 139:3648–3666. doi:10.1175/MWR-D-11-00004.1

Penland C (1989) Random forcing and forecasting using principal oscillation pattern analysis. Mon Weather Rev 117:2165–2185

Penland C, Magorian T (1993) Prediction of Nino 3 sea surface temperatures using linear inverse modeling. J Clim 6:1067–1076

Penland C, Matrosova L (1994) A balance condition for stochastic numerical models with application to the El Nino-southern oscillation. J Clim 7:1352–1372

Penland C, Sardeshmukh P (1995) The optimal growth of tropical sea surface temperature anomalies. J Clim 8:1999–2024

Perron M, Sura P (2013) Climatology of non-gaussian atmospheric statistics. J Clim 26:1063–1083. doi:10.1175/JCLI-D-11-00504.1

Reichler T, Roads J (2005) Long-range predictability in the tropics. Part II: 30–60-day variability. J Clim 18:634–650

Roundy PE, Gribble-Verhagen LM (2010) Variations in the flow of the global atmosphere associated with a composite convectively coupled oceanic kelvin wave. J Clim 23:4192–4201. doi:10.1175/2010JCLI3630.1

Straub KH (2013) MJO initiation in the real-time multivariate MJO index. J Clim 26:1130–1151. doi:10.1175/JCLI-D-12-00074.1

Subramanian AC, Jochum M, Miller AJ et al (2011) The Madden–Julian Oscillation in CCSM4. J Clim 24:6261–6282. doi:10.1175/JCLI-D-11-00031.1

Sura P, Newman M, Penland C, Sardeshmukh P (2005) multiplicative noise and non-gaussianity: a paradigm for atmospheric regimes? J Atmos Sci 62:1391–1409. doi:10.1175/JAS3408.1

Vitart F, Leroy A, Wheeler MC (2010) A comparison of dynamical and statistical predictions of weekly tropical cyclone activity in the southern hemisphere. Mon Weather Rev 138:3671–3682. doi:10.1175/2010MWR3343.1

Von Storch H, Xu J (1990) Principal oscillation pattern analysis of the 30- to 60-day oscillation in the tropical troposphere. Clim Dyn 4:175–190

Waliser D, Jones C (1999) A statistical extended-range tropical forecast model based on the slow evolution of the Madden–Julian Oscillation. J Clim 12:1918–1939

Waliser D, Moncrief M (2007) The Year of Tropical Convection (YOTC) Science plan: a joint WCRP-W WRP/THORPEX International Initiative. WMO/TD No. 1452, WCRP-130, WWRP/THORPEX-No 9. WMO, Geneva, Switzerland, pp 1–24

Waliser DE, Stern W, Schubert S, Lau KM (2003) Dynamic predictability of intraseasonal variability associated with the Asian summer monsoon. Q J R Meteorol Soc 129:2897–2925. doi:10.1256/qj.02.51

Wallace J, Gutzler D (1981) Teleconnections in the geopotential height field during the northern hemisphere winter. Mon Weather Rev 109:784–812

Wheeler MC, Hendon HH (2004) An all-season real-time multivariate MJO index: development of an index for monitoring and prediction. Mon Weather Rev 132:1917–1932. doi:10.1175/1520-0493(2004)132<1917:AARMMI>2.0.CO;2

Wheeler M, Weickmann K (2001) Real-time monitoring and prediction of modes of coherent synoptic to intraseasonal tropical variability. Mon Weather Rev 129:2677–2694

Winkler C (2001) A linear model of wintertime low-frequency variability. Part I: formulation and forecast skill. J Clim 14:4474–4494. doi:10.1175/1520-0442(2001)014<4474:ALMOWL>2.0.CO;2

Yoneyama K, Zhang C, Long C (2013) Tracking pulses of the Madden–Julian Oscillation. Bull Am Meteorol Soc. doi:10.1175/BAMS-D-12-00157.1

Zhang C (2001) Intraseasonal perturbations in sea surface temperatures of the equatorial eastern pacific and their association with the Madden–Julian Oscillation. J Clim 14:1309–1322

Zhang C, Gottschalck J, Maloney ED et al (2013) Cracking the MJO nut. Geophys Res Lett 40:1223–1230. doi:10.1002/grl.50244